Endocr (2011) 39:104–112
DOI 10.1007/s12020-010-9418-1

ORIGINAL ARTICLE

Loss-of-function of SHARPIN causes an osteopenic phenotype in mice

Tian Xia · Yanhua Liang · Junrong Ma · Mi Li · Meng Gong · Xijie Yu

Received: 17 June 2010 / Accepted: 22 October 2010 / Published online: 11 November 2010

Abstract SHARPIN is a novel protein thought to interact with SHANK family and is widely expressed in multiple tissues/cells, including osteoblasts and osteoclasts. Loss-of-function of *Sharpin* develops the chronic proliferative dermatitis mutation (CPDM) in mice as well as a severe inflammation in other organs. The actual function of SHARPIN is poorly understood. Our aim was to determine the functional roles of SHARPIN in bone metabolism by using CPDM mice. The skeletal phenotypes were determined by peripheral quantitative computed tomography, micro-computed tomography, and quantitative real-time RT-PCR, the cellular functions of osteoblasts and osteoclasts were investigated by ex vivo cell culture. Compared to wild-type controls, CPDM mice demonstrated significantly lower total and cortical bone mineral content and bone mineral density, trabecular and cortical bone volume, and trabecular number. The mRNA expression of Runx2, osterix, type I collagen, and osteocalcin was significantly lower in the bone from CPDM mice. Osteoclasts and osteoblasts from CPDM mice were functionally defective. Our result suggests that SHARPIN plays important regulating roles in bone metabolism. These functional roles may either come from systemic chronic inflammatory or directly signaling pathway within bone cells.

Keywords SHARPIN · Osteopenia · Osteoblasts · Osteoclasts

Introduction

The *Sharpin* gene is located on chromosome 15 in mice, chromosome 8 in human, and conserved in human, chimpanzee, dog, cow, rat, and zebrafish (http://www.ncbi.nlm.nih.gov/gene/). The encoded protein, SHARPIN, is a novel protein and widely expressed in multiple tissues with the highest level in immune cells (NK cells, B cells, and mast cells), testis, and heart [1] (http://biogps.gnf.org/). SHARPIN is an intracellular cytoplasm protein and predicted to be a protein of 380 amino acids with the exon 8 splice variant encoding 315 amino acids. Although the predicted protein does not show extensive homology with other known proteins, three previously defined motifs are present, such as the Hoil1-N domain of ubiquitin-protein ligase activity, region AA172–305 interacting with SHANK, and C terminal zinc finger domain [2]. The actual function of SHARPIN is largely unknown. SHARPIN protein forms homodimers and associates with SHANK in the post-synaptic density of excitatory neurotransmitters in the brain. SHARPIN is hypothesized to have roles in the cross-linking of SHANK proteins and is associated with neurological signaling [3]. SHARPIN has also been identified as a commonly up-regulated gene in multiple human cancer types. Chinese ovary hamster cells over expressing SHARPIN exhibited enhanced cancer-specific phenotypes in multiple in vitro tumor assays. These results suggest that

Tian Xia and Yanhua Liang contribute equally to this work.

T. Xia · J. Ma · M. Li · X. Yu (✉)
Laboratory of Endocrinology and Metabolism, West China Hospital, Sichuan University, No. 37, Guoxue Xiang, 610041 Chengdu, People's Republic of China
e-mail: xijieyu@hotmail.com

M. Gong · X. Yu
Maine Institute for Human Genetics & Health, Bangor, ME 04401, USA

Y. Liang
Department of Dermatology, Yale University School of Medicine, New Haven, CT 06511, USA

SHARPIN may play tumor-associated roles during cancer biogenesis [4]. SHARPIN is expressed in bone, osteoblasts, and osteoclasts [1] (http://biogps.gnf.org/), but its functional roles in bone development and metabolism have not been explored.

Loss-of-function of SHARPIN was identified as the genetic basis of the chronic proliferative dermatitis mutation (CPDM) in mice [5]. A single base pair deletion in the 3′end of exon 1 creates a shift in the open reading frame predicted to cause a premature stop codon at position 624 [5]. CPDM is an autosomal recessive, spontaneous, and systemic inflammatory disorder. Mice homozygous for this spontaneous mutation develop a severe, chronic, and inflammatory skin disease beginning at 3–5 weeks of age. The skin lesions were described as "psoriasiform dermatitis" in that the mice develop inflamed, scaly skin, and somewhat reminiscent of psoriasis [6–10]. In addition to dermatitis, homozygotes exhibit multi-organ inflammation with eosinophilia, defective TH1 cytokine production, splenomegaly, absent Peyer's patches (adult), diminished serum immunoglobulins, and an absence of B cell follicles, follicular dendritic cells, and germinal centers in secondary lymph organs [11]. Many of the chronic inflammatory diseases are associated with systemic bone loss [12]. Interestingly, CPDM mice show moderate growth retardation with aging [6]. CPDM mice also exhibit weight reduction from age of 5 weeks (7%) and reduction of 12% has been observed at 6 weeks [9]. Growth retardation usually means abnormalities in skeletal development and/or metabolism. Here, we use CPDM mice as model to study the skeletal phenotype. Our research reveals that loss-of-function of SHARPIN results in an osteopenic phenotype in mice.

Results

Osteopenic phenotype in CPDM mice

Since CPDM mice show growth retardation and weight reduction from the age of 5 weeks [6], we studied skeletal phenotype in mature mice at the age of 10 weeks. Compared to wild-type controls, CPDM mice showed significant shorter femur (13.489 ± 0.144 vs. 14.532 ± 0.208, $P < 0.05$). Volumetric bone densitometry in femur was studied by peripheral quantitative computed tomography (pQCT). CPDM mice showed significantly lower total bone mineral content (BMC) (less than 48%, $P < 0.001$) and cortical BMC (48% less, $P < 0.001$), total bone mineral density (BMD) (28% less, $P < 0.001$), as well as cortical BMD (about 7% less, $P < 0.05$) (Table 1). In the midshaft area, CPDM mice showed 24% less in cortical thickness ($P < 0.001$) and 5% less in periosteal

Table 1 Bone mass studied by pQCT

Genotype	Total BMC (mg)	Total vol. (cm^3)	Total BMD (mg/cm^3)	Cort. BMC (mg)	Cort. vol. (cm^3)	Cort. BMD (mg/cm^3)	Cort. Thick. (mm)	Peri C (mm)	Endo C (mm)
WT($n = 10$)	7.33 ± 0.326	15.162 ± 0.432	0.483 ± 0.00903	4.758 ± 0.2555	4.508 ± 0.227	1.055 ± 0.00817	0.156 ± 0.0043	4.802 ± 0.0846	3.823 ± 0.0629
CPDM ($n = 10$)	4.945 ± 0.153***	14.17 ± 0.459	0.349 ± 0.00688***	2.5075 ± 0.0569***	2.561 ± 0.0511*	0.979 ± 0.00292*	0.119 ± 0.00236***	4.538 ± 0.0667*	3.789 ± 0.0781

Left femurs of male WT and CPDM mice (CPDM) were measured for bone mass with the SA Plus densitometer. Compared to wild-type controls, CPDM mice showed significantly lower total BMC (48% less, $P < 0.001$) and cortical BMC (48% less, $P < 0.001$), total BMD (28% less, $P < 0.001$) as well as cortical BMD (7% less, $P < 0.05$). CPDM mice showed 24% reduction in cortical thickness ($P < 0.001$) and 5% reduction in periosteal circumference ($P < 0.05$) (compared to WT, * $P < 0.05$, ** $P < 0.01$, *** $P < 0.001$)

circumference ($P < 0.05$) (Table 1). These results indicate that CPDM mice have a shorter bone with reduced BMD and BMC.

We then studied bone volume and bone structure for the same bones by micro-computed tomography (μCT). Compared to wild-type controls, CPDM mice showed 21% less in trabecular BV/TV ($P < 0.01$), 12% less in cortical BV/TV ($P < 0.05$) (Table 2, Fig. 1). We then studied bone morphometry of distal femur metaphyseal trabecular bone. CPDM mice showed significant lower trabecular number (18% less, $P < 0.01$), but higher trabecular space (25% higher, $P < 0.01$) (Table 2, Fig. 1). These data are consistent with pQCT data, which indicates that loss-of-function of *Sharpin* causes an osteopenic phenotype in CPDM mice.

Abnormal gene expression in the bone of CPDM mice

We studied bone-related gene expression in distal femur metaphyseal region, which is enriched of osteoprogenitors. We isolated total RNA and used real-time qRT-PCR to investigate gene expression. Compared to wild-type mice, CPDM mice showed significant lower mRNA expression of Runx2 (50% less, $P < 0.001$, Fig. 2), which is a member of the RUNX family of transcription factors and has a Runt DNA-binding domain. Runx2 is essential for osteoblastic differentiation and skeletal morphogenesis, and acts as a scaffold for nucleic acids and regulatory factors involved in skeletal gene expression [13]. CPDM mice also showed significant lower mRNA expression of osterix (70% less, $P < 0.001$, Fig. 2), a novel zinc finger containing transcription factor that is regulated by Runx2 and is essential for osteoblast differentiation [14]. The mRNA expression of osteocalcin was significantly lower in CPDM mice (75% less, $P < 0.001$, Fig. 2). Osteocalcin is secreted solely by osteoblasts and it is often used as a biomarker for the bone formation process [15]. mRNA expression of type I collagen, the most abundant collagen in bone, was also significantly lower in CPDM mice (60% less, $P < 0.001$, Fig. 2). Our result indicates that loss-of-function of *Sharpin* impairs bone-related gene expression, which may be responsible for osteopenic phenotype in CPDM mice.

Table 2 Bone mass studied by μCT

Genotype	Tb. BV/TV (%)	Tb.N (1/mm)	Tb.Th (mm)	Tb.Sp (mm)	Cort BV/TV (%)
WT ($n = 10$)	0.0361 ± 0.002	3.597 ± 0.111	0.0391 ± 0.001	0.280 ± 0.009	0.477 ± 0.005
CPDM ($n = 10$)	0.0284 ± 0.002**	2.938 ± 0.230**	0.0386 ± 0.001	0.352 ± 0.026**	0.419 ± 0.008*

Left femurs of male wild-type (WT) and CPDM mice (CPDM) were measured for density using MicroCT40. Compared to wild-type controls, CPDM mice showed 21% reduction in trabecular BV/TV ($P < 0.01$), 12% reduction in cortical BV/TV ($P < 0.05$). CPDM mice showed significant lower trabecular number (18% reduction, $P < 0.01$), but higher trabecular space (25% increased, $P < 0.01$) (compared to WT, * $P < 0.05$, ** $P < 0.01$, *** $P < 0.001$)

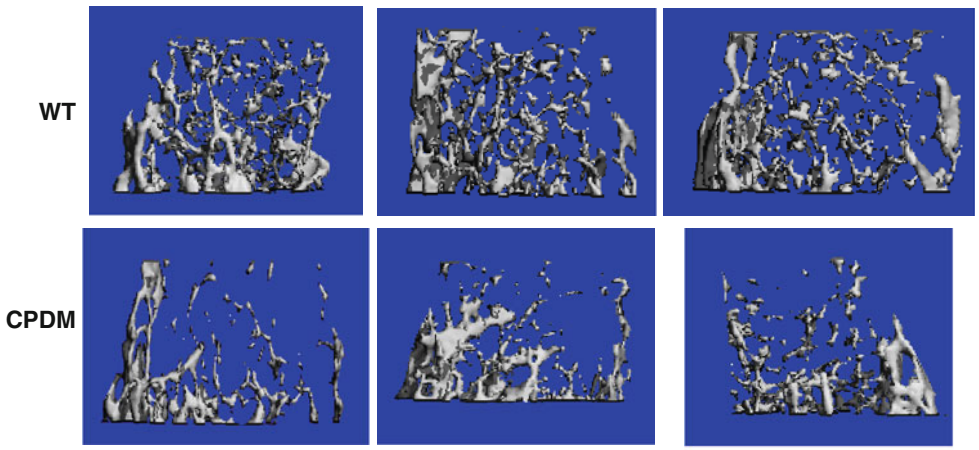

Fig. 1 Bone structure studied by μCT. Left femurs were scanned by μCT at approximately 0.6 mm proximal to the growth plate to investigate trabecular bone structure. The scanning extended proximally 1.5 mm. One hundred fifty cross-sectional slices were made at 12 μm intervals at the distal end beginning at the growth plate side and extending in a proximal direction, and then 100 contiguous slices were selected for analysis. Compared to wild-type mice, CPDM mice showed less trabecular number as well as bone volume ($n = 3$ for each group)

Abnormal ex vivo osteoblast and osteoclast function in CPDM mice

We have found lower BMD and bone volume, as well as abnormal skeletal related gene expression in CPDM mice. As SHARPIN is expressed widely and may play function in multiple organs and systems. The abnormal skeletal phenotypes in CPDM mice may come from the direct effect of SHARPIN on bone; it may also be the consequence of the defects in other organs or systems. We studied ex vivo osteoblast and osteoclast functions to exclude the possible effect from other organs and systems.

Ex vivo osteoclast culture showed that there were less osteoclasts induced from CPDM bone marrow. The cellular size was much smaller, and the nuclei were less in osteoclasts from CPDM mice (Fig. 3). As the size and nuclei number were correlated with osteoclastic function, this result indicated that loss-of-function in *Sharpin* significantly decreased osteoclast formation and function. There was no difference in total cell number (TRAP positive plus TRAP negative cells) between CPDM and wild-type osteoclast cultures (data not shown), which indicated abnormalities in CPDM osteoclasts resulted from the reason other than abnormal proliferation.

We then did ex vivo osteoblast culture from bone marrow stromal cells (BMSCs). Followed by the standard protocol, BMSCs were cultured under regular medium for the first week to keep proliferation. There was no significant difference in cellular proliferation between wild-type and CPDM mice during proliferate period (Fig. 4a). The BMSCs were induced to differentiate into mature osteoblast under osteoblastic conditional medium from the second week to the fourth week. By the end of osteoblastic culture, osteoblasts induced from CPDM mice showed significantly less area of Von Kossa positive, an index for in vitro bone mineral formation (Fig. 4b). This result indicated that SHARPIN may directly regulate osteoblast mineralization, but not proliferation.

Discussion

SHARPIN is a novel protein thought to interact with SHANK family proteins [3]. The functional roles of SHARPIN in bone metabolism are unknown. In the present study, we used CPDM mice as a model to investigate the skeletal phenotypes without SHARPIN. We found that loss-of-function mutation in SHARPIN in mice caused an osteopenic phenotype. Further mechanism studies revealed that the expression of bone-related genes (Runx2, osterix, osteocalcin, and type I collagen) was significantly lower in CPDM mice bone. Ex vivo cell culture showed osteoclasts and osteoblasts from CPDM mice were functionally defective. Our result indicates that SHARPIN plays important regulating roles in bone metabolism.

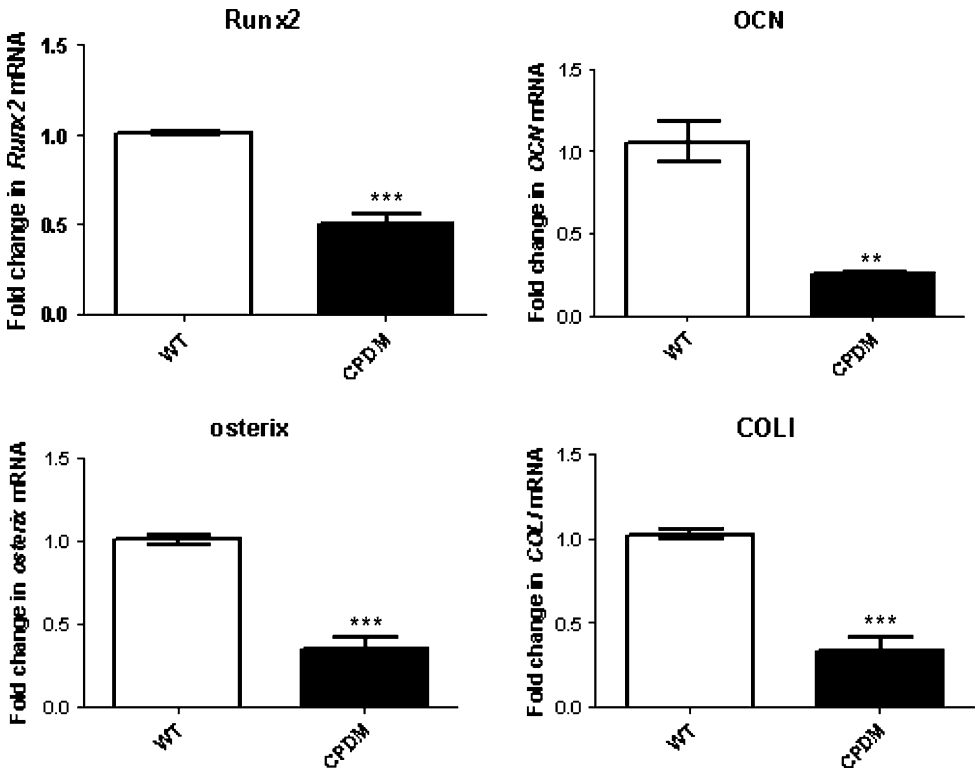

Fig. 2 Abnormal mRNA expression profile in CPDM bone. Total RNA was isolated from is metaphyses of right femurs. mRNA expression of bone related genes was studied by real-time qRT-PCR. CPDM mice showed significantly lower mRNA expression of Runx2, osterix, osteocalcin (OCN), and type I collagen (COLI) ($n = 10$, compared to wild-type, ** $P < 0.01$, *** $P < 0.001$)

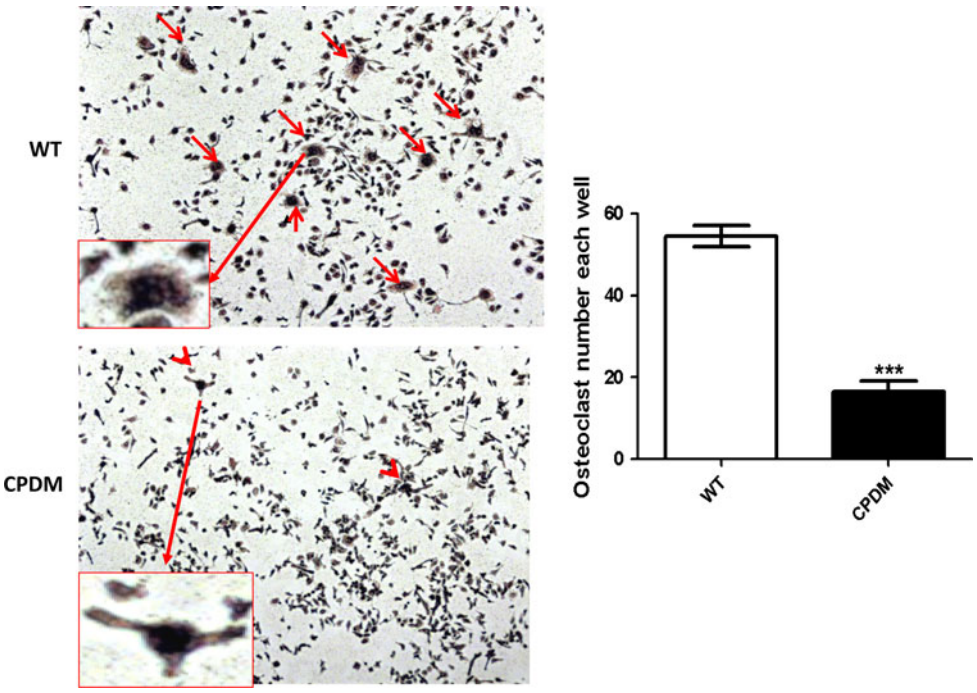

Fig. 3 Less osteoclast formation from CPDM mice. Bone marrow cells from tibias of CPDM and WT mice were cultured in the presence of human soluble RANKL at 30 ng/mL and recombinant mouse M-CSF at 25 ng/mL for 7 days to induce osteoclast formation. Cultured cells were stained for TRAP. TRAP positive multinucleated (containing three or more nuclei, shown as *zoomed image* for wild-type and CPDM culture) cells were classified as osteoclasts. A *zoomed in* image for a single multinucleated osteoclast was shown in the *bottom* of both wild-type and CPDM culture image. The osteoclast number was less and the cellular size was smaller in CPDM mice than that in WT mice ($n = 8$, compared to wild-type, *** $P < 0.001$)

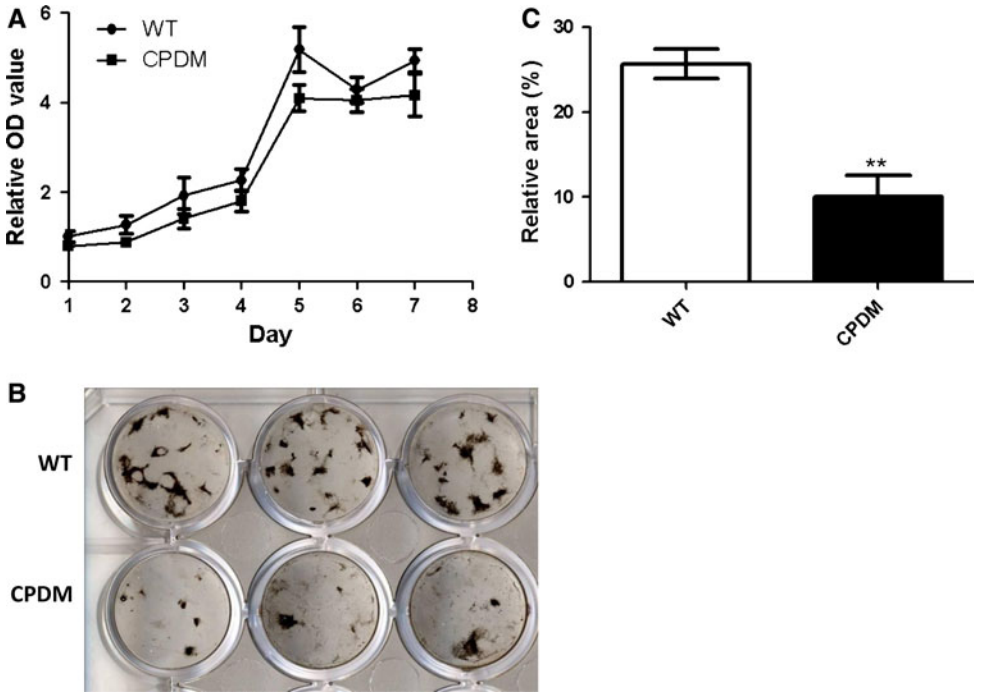

Fig. 4 Defect in mineralization in CPDM osteoblasts. BMSCs from tibias of CPDM and WT mice were cultured in regular medium for 7 days to reach confluence. **a** The cellular proliferation in regular medium was further studied by MTT assay. There was no difference in cellular proliferation in BMSCs between WT and CPDM. **b** The medium was changed to osteoblastic medium from the second week to the fourth week to induce differentiation. In vitro bone mineral formation was investigated by Von Kossa staining. **c** Bioquant Osteo II software was used to analyze staining area. The data was presented as ratio of the positive staining area to the total area. Osteoblasts from CPDM mice showed significantly less area of mineralization ($n = 3$, compared to wild-type, ** $P < 0.01$)

On the molecular basis of the abnormal skeletal phenotype in CPDM mice, there may have few possibilities. First, many of the chronic inflammatory diseases have been reported to associate with systemic bone loss. Bone loss was due to direct effects of inflammation, poor nutrition, reduced lean body mass, immobility, and the effects of

treatments, such as glucocorticoids [12]. Systemic Inflammatory cytokines such as interleukin family members (IL-1β, IL-6, and IL-11), tumor necrosis factor-alpha (TNF-α), granulocyte-macrophage colony-stimulating factor (G-MCF) could directly affect bone resorption and/or bone formation leading to bone loss [16, 17]. Bone was also very sensitive to nutritional state. Most chronic inflammatory diseases were associated with a catabolic state that favored the loss-of lean mass and this reduced bone formation. Diseases that affect the gastrointestinal tract would have an additional impact on the intake of nutrients and calories [12]. CPDM mice developed a multi-organ inflammation with eosinophilia in skin, joint [6], lung, lymph node, and stomach [9]. There was increased expression of IL-4, IL-5, IL-13, and G-MCF in the skin of CPDM mice. Supernatants of cultured spleen cells of CPDM mice contained an increased amount of IL-5 and IL-13, and a decreased amount of IFN-γ [18]. These systemic inflammatory cytokines may directly affect bone metabolism in CPDM mice. On the other hand, esophageal and stomach inflammation in CPDM mice may directly reduce the intake of nutrients and calories [9], which could further worsen bone metabolism.

Second, recent research has found that the epidermis can act as an endocrine-like organ to regulate bone metabolism. Low bone mineral density was found in adult patients with moderate to severe atopic dermatitis, a chronic inflammatory skin disease [19]. Animal study showed when JunB was constitutively deleted from epidermal keratinocytes, a multi-organ disease developed affecting the skin, the hematopoietic system as well as the bone compartment [20]. The phenotype of $JunB^{\Delta ep}$ mice (JunB was constitutively deleted from epidermal keratinocytes) was very similar with that of CPDM mice. Adult $JunB^{\Delta ep}$ mice developed severe skin ulcerations at 2–3 months of age. Skin lesions showed characteristics of epidermal thickening (acanthosis) with pronounced infiltrations of granulocytes, lymphocytes, and mast cells [20]. Similar to CPDM mice, $JunB^{\Delta ep}$ mice had enlarged spleens and lymph nodes containing up to a tenfold increase in cell numbers. In addition, cellular granulocytes were present in other organs, including the liver and bone marrow [20]. Of note, both mice developed a similar osteopenic phenotype at the age of 2–3 months accompanying with reduced osteoclast formation and osteocalcin expression. Intriguingly, G-CSF was shown to be a direct transcriptional target of JunB. Similar to CPDM mice, mutant epidermis from $JunB^{\Delta ep}$ mice released large amounts of G-CSF and caused skin ulcerations, myeloproliferative disease, and low bone mass [20]. Based on low BMD in atopic dermatitis, and the highly similar phenotypes between $JunB^{\Delta ep}$ mice and CPDM mice, we speculated that similar signaling pathway may exist in CPDM mice, which may communicate between epidermis and skeleton to regulate bone metabolism.

Third, SHARPIN is expressed osteoblasts and osteoclasts. Our ex vivo cell culture demonstrated that there were lower osteoclastic formation and osteoblastic mineralization in CPDM mice. Since the systemic factors were excluded in the cell culture system, our research result indicated that SHARPIN might directly regulate the formation and function of osteoclast and osteoblast. However, we could not completely exclude indirect function from other systems by using this general knockout mouse model. A conditional knockout SHARPIN in osteoblasts/osteoclasts is required to answer this question.

In summary, we found an osteopenic phenotype in mice lack of SHARPIN. SHARPIN may directly target osteoblast/osteoclast, or through the inflammation in multiple organs, or epidermis acting as an endocrine-like organ, to regulate bone metabolism.

Materials and methods

Animals for study

cpdm/cpdm (CPDM) mice on a C57BL/KaLawRij background were purchased from The Jackson Laboratory (Bar Harbor, ME) and maintained under conventional conditions. Followed by vender's instruction, breeding was done by mating heterozygotes. The genotyping assay was run on the Biotage PSQ 96MA by using pyrosequencing technology. All animal protocols were approved by Animal Care and Use Committee. Age-matched CPDM male mice and their wild-type male littermates were used when aged 10 weeks for in vivo and in vitro studies. Mice were housed under standard conditions of 12:12 h light/dark cycle, with water and food ad libitum (Purina Rodent lab Chow 5001, containing 0.95% Ca, 0.67% P, and vitamin D3 4500 IU/kg). Mice were euthanized by CO_2 inhalation plus thoracic transection to assure death.

pQCT for volumetric bone densitometry

pQCT was used to measure volumetric BMD (vBMD) on the left femur of male wild-type (WT) and CPDM mice at 10 week of age. Isolated femur lengths were measured with digital calipers (Stoelting, Wood Dale, IL), and then femurs were measured for density using the SA Plus densitometer (Orthometrics, White Plains, NY). Calibration of the SA Plus instrument was accomplished with a manufacturer-supplied phantom and with hydroxyapatite standards of known density (50–1000 mg/mm^3) with cylindrical dimensions (2.4 mm diameter $\times$ 24 mm length) that approximate mouse femurs. Accuracy of linear measures

was checked with defined thickness of aluminum foils. The bone scans were analyzed with thresholds of 710 and 570 mg/cm^3; using Orthometrics software version 5.50 yielding cortical bone areas that were consistent with histomorphometrically derived periosteal values. Mineral content was determined with thresholds of 220 and 400 mg/cm^3, selected so that mineral from most partial voxels (0.07 mm) would be included in the analysis. Precision of the SA Plus for repeated measurement of a single femur was found to be within 1.2–1.4%. Isolated femurs were scanned at seven locations at 2 mm intervals, beginning 0.8 mm from the distal ends of the epiphyseal condyles. Total vBMD values were calculated by dividing the total mineral content by the total bone volume and expressed as milligrams per cubic millimeter. Cortical thickness was obtained at the midshaft scan.

μCT40 for femur distal trabecular bone macro-structure and bone volume

Trabecular bone components of left distal femur were measured by μCT (MicroCT40, Scanco Medical AG, Bassersdorf, Switzerland). This instrument provides high-resolution data for trabecular bone volume as well as trabecular number, thickness, and spacing. The MicroCT40 unit is calibrated weekly with a phantom standard provided by Scanco. Femurs from CPDM mice and WT control mice at 10 week of age were scanned for microarchitecture in the metaphyseal region of the distal femur. The femurs were scanned at the energy level of 55 keV, and intensity of 177 μA. The distal trabecular scan started about 0.6 mm proximal to the growth plate and extended proximally 1.5 mm. One hundred fifty cross-sectional slices were made at 12 μm intervals at the distal end beginning at the growth plate side and extending in a proximal direction, and then 100 contiguous slices were selected for analysis. These were contoured inside the endocortical edge of the cortical shell to obtain the total volume (TV) of the space, followed by analysis of the trabecular bone volume (BV) with the Scanco software version 5.0.

Real-time qRT-PCR for bone related gene expression

Right femur distal metaphyses from CPDM mice and WT control mice at 10 week of age were resected and chopped finely with a scalpel. This region is highly enriched for committed osteoprogenitors [21]. Bone pieces were homogenized in Trizol with a Tissue-Tearor (BioSpec Products Inc., Bartlesville, OK). RNA was extracted from bone using the RNeasy RNA kit (Qiagen, Inc., Valencia, CA).

The TaqMan primers and probes for mouse type I collagen, Runx2, osteocalcin, osterix, and β-actin were designed using Primer Express software (Applied Biosystems, Foster City, CA). The primers and probes were designed to span at least one intron to eliminate non-specific signals due to genomic DNA amplification. RT and real-time quantitative PCR were performed in a one-step reaction using the TaqMan Gold RT-PCR kit and protocols provided by the manufacturer (Applied Biosystems). Briefly, a typical reaction contained 50 ng total RNA and 1.25 U of Gold DNA polymerase, 12.5 U of MultiScribe Reverse Transcriptase, and 5.5 mM $MgCl_2$ in a 50 μl reaction volume. Primers and TaqMan probes were added at a final concentration 200 and 100 nM, respectively. The dNTP final concentration was 0.3 mM each except for dUTP, which was 0.6 mM. Amplification was performed in ABI 7500 Sequence Detection System (Applied Biosystems). The thermal cycling protocol consisted of RT at 48°C for 30 min and activation of Gold DNA polymerase at 95°C for 5 min, followed by 40 cycles of template denaturing at 95°C for 15 s and annealing/extension at 60°C for 1 min. Accumulation of the PCR products was detected by directly monitoring the increase in fluorescence of the reporter dye. The mean of the background fluorescence emission for all tested wells measured between cycles 3 and 14 used to set the baseline. A threshold for the amplification of each gene of interest was then established by drawing a line that intersected the exponential phase of the logarithmic amplification curves for all samples being analyzed for the expression of the target gene. All primer sets were tested for specific amplification of mRNA by parallel analyses of controls that included omitting RT or template and resulted in no fluorescent signal detection. Each RNA sample was analyzed in triplicate, and each experiment was performed independently at least three times. The amplification of bone genes and β-actin was equally efficient, and the $2^{-\Delta\Delta CT}$ method described by Livak and Schmittgen [22] was used to analyze the data. The expression level of mRNA in CPDM mice was calculated relative to that in wild-type mice.

In vitro osteoclast culture

Tibias from CPDM mice and WT control mice at 10 week of age were used for osteoclast culture. Bone marrow cells were cultured at a density of 1 × 106 cells/well in a 24 well plate. The cells were treated with human soluble RANKL (30 ng/ml, PeproTech, Inc., Rocky Hill, NJ) and rmM-CSF (25 ng/ml, PeproTech, Inc., Rocky Hill, NJ). The cells were cultured for 8 days with a medium change every 3 days with fresh sRANKL and rmM-CSF. The cells were fixed with 4% paraformaldehyde for 30 min at RT on the last day, rinsed with DI water. The cells were air dried well for TRAP staining.

TRAP staining

Osteoclasts were rinsed with 1×PBS for three times. The cells were then incubated with TRAP solution at 37°C for 1 h. TRAP solution formula was listed below: fast GBC solution 67 μl, sodium nitrite 67 μl, ASBI 67 μl, Acetate solution 267 μl, and Tartrate 133 μl. Mix fast GBC solution and sodium nitrite gently and stay for 2 min. The cells were washed with ddH_2O after staining. The staining was visualized under a Zeiss Axiovert 200 M microscope. TRAP positive multinucleated (containing three or more nuclei) cells were classified as osteoclasts.

In vitro osteoblast culture

Tibias from CPDM mice and WT control mice at 10 week of age were used for bone marrow stromal cell culture. Bone marrow was flushed out from the tibias with a 3 cc syringe and 25G needle. BMSC were cultured in plate or dish at a density of 1.5×10^4 cells/cm^2 in α-MEM (Invitrogen, Carlsbad, CA) containing 10% FBS, 1% penicillin, 1% streptomycin, 1% L-glutamine, and 1% non-essential amino acids. The day of plating was counted as day zero. At day 2, medium was refreshed to remove cells that were not attached to culture plate. Plated cells became confluent around days 5–6; and then at day 7 the culture medium was changed to osteoblastic differentiation medium, which consisted of regular medium plus 50 μg/ml ascorbic acid and 10 mM glycerophosphate. Medium was changed every other day for the entire duration of culture. At day 28, the cells were washed with 1×PBS and fixed with 4% paraformaldehyde for 10 min for Von Kossa staining.

MTT assay

BMSC culture at day 7 was digested with 0.05% trypsin, BMSCs were then plated in 96-well plates at a density of 1,000 cells/well overnight to allow attachment. After serum starvation for 12 h, medium was replaced with 100 μl fresh medium containing 0.5 mg/ml MTT at the indicated time points. After 4 h incubation, medium was removed and purple blue sediment was dissolved in 150 μl DMSO. The relative optical density (OD) for each well was determined using a WELLSCAN MK3 ELISA kit (Labsystems, Dragon, Finland).

Von Kossa mineralization staining

The fixed cells were rinsed with water, and exposed to 2 ml of 5% silver nitrate solution for 1 h with strong light. The cells were rinsed with water. 2 ml 5% sodium thiosulfate solution was added to cells for 2–3 min, the cells were then rinsed with water and air dried. The staining was visualized under a Zeiss Axiovert 200 M microscope. Bioquant OsteoII software (BIOQUANT Image Analysis Corporation, Nashville, TN) was used to analyze staining area. The data were presented as ratio of the positive staining area to the total area.

Statistical analyses

Analyses were performed with JMP 8.0 software (SAS Inc., Cary, NC). Unpaired *t*-tests were used to compare two groups (CPDM vs. WT). Differences were considered statistically significant at $P < 0.05$ on a two-tailed test. Data were expressed as means ± standard error of the mean (SEM).

Acknowledgment This work was support by a grant to Dr. Xijie Yu from National Natural Science Foundation of China (No. 30872632).

References

1. Y. Daigo, I. Takayama, S.M. Ward, K.M. Sanders, M.A. Fujino, Novel human and mouse genes encoding a shank-interacting protein and its upregulation in gastric fundus of W/WV mouse. J. Gastroenterol. Hepatol. **18**, 712–718 (2003)
2. A. Marchler-Bauer, J.B. Anderson, M.K. Derbyshire, C. DeWeese-Scott, N.R. Gonzales, M. Gwadz, L. Hao, S. He, D.I. Hurwitz, J.D. Jackson, Z. Ke, D. Krylov, C.J. Lanczycki, C.A. Liebert, C. Liu, F. Lu, S. Lu, G.H. Marchler, M. Mullokandov, J.S. Song, N. Thanki, R.A. Yamashita, J.J. Yin, D. Zhang, S.H. Bryant, CDD: a conserved domain database for interactive domain family analysis. Nucleic Acids Res. **35**, D237–D240 (2007)
3. S. Lim, C. Sala, J. Yoon, S. Park, S. Kuroda, M. Sheng, E. Kim, Sharpin, a novel postsynaptic density protein that directly interacts with the shank family of proteins. Mol. Cell Neurosci. **17**, 385–397 (2001)
4. J. Jung, J.M. Kim, B. Park, Y. Cheon, B. Lee, S.H. Choo, S.S. Koh, S. Lee, Newly identified tumor-associated role of human Sharpin. Mol. Cell. Biochem. **340**, 161–167 (2010)
5. R.E. Seymour, M.G. Hasham, G.A. Cox, L.D. Shultz, H. Hogenesch, D.C. Roopenian, J.P. Sundberg, Spontaneous mutations in the mouse Sharpin gene result in multiorgan inflammation, immune system dysregulation and dermatitis. Genes Immun. **8**, 416–421 (2007)
6. H. HogenEsch, M.J. Gijbels, E. Offerman, J. van Hooft, D.W. van Bekkum, C. Zurcher, A spontaneous mutation characterized by chronic proliferative dermatitis in C57BL mice. Am. J. Pathol. **143**, 972–982 (1993)
7. H.I. Gallardo Torres, M.J. Gijbels, H. HegnEsch, G. Kraal, Chronic proliferative dermatitis in mice: neutrophil-endothelium interactions and the role of adhesion molecules. Pathobiology **63**, 341–347 (1995)
8. M.J. Gijbels, H. HogenEsch, B. Blauw, P. Roholl, C. Zurcher, Ultrastructure of epidermis of mice with chronic proliferative dermatitis. Ultrastruct. Pathol. **19**, 107–111 (1995)
9. M.J. Gijbels, C. Zurcher, G. Kraal, G.R. Elliott, H. HogenEsch, G. Schijff, H.F. Savelkoul, P.L. Bruijnzeel, Pathogenesis of skin lesions in mice with chronic proliferative dermatitis (cpdm/cpdm). Am. J. Pathol. **148**, 941–950 (1996)

10. H. HogenEsch, D. Boggess, J.P. Sundberg, Changes in keratin and filaggrin expression in the skin of CPDM mutant mice. Pathobiology **67**, 45–50 (1999)
11. H. HogenEsch, S. Janke, D. Boggess, J.P. Sundberg, Absence of Peyer's patches and abnormal lymphoid architecture in chronic proliferative dermatitis (cpdm/cpdm) mice. J. Immunol. **162**, 3890–3896 (1999)
12. R. Hardy, M.S. Cooper, Bone loss in inflammatory disorders. J. Endocrinol. **201**, 309–320 (2009)
13. T.M. Schroeder, E.D. Jensen, J.J. Westendorf, Runx2: a master organizer of gene transcription in developing and maturing osteoblasts. Birth Defects Res. C Embryo Today **75**, 213–225 (2005)
14. K. Nakashima, X. Zhou, G. Kunkel, Z. Zhang, J.M. Deng, R.R. Behringer, B. de Crombrugghe, The novel zinc finger-containing transcription factor osterix is required for osteoblast differentiation and bone formation. Cell **108**, 17–29 (2002)
15. C. Desbois, G. Karsenty, Osteocalcin cluster: implications for functional studies. J. Cell Biochem. **57**, 379–383 (1995)
16. J. Lorenzo, M. Horowitz, Y. Choi, Osteoimmunology: interactions of the bone and immune system. Endocr. Rev. **29**, 403–440 (2008)
17. L. Gilbert, X. He, P. Farmer, S. Boden, M. Kozlowski, J. Rubin, M.S. Nanes, Inhibition of osteoblast differentiation by tumor necrosis factor-alpha. Endocrinology **141**, 3956–3964 (2000)
18. M.L. Renninger, R. Seymour, J.W. Lillard Jr., J.P. Sundberg, H. HogenEsch, Increased expression of chemokines in the skin of chronic proliferative dermatitis mutant mice. Exp. Dermatol. **14**, 906–913 (2005)
19. I.M. Haeck, N.A. Hamdy, L. Timmer-de Mik, E.G. Lentjes, H.J. Verhaar, M.J. Knol, M.S. de Bruin-Weller, C.A. Bruijnzeel-Koomen, Low bone mineral density in adult patients with moderate to severe atopic dermatitis. Br. J. Dermatol. **161**, 1248–1254 (2009)
20. A. Meixner, R. Zenz, H.B. Schonthaler, L. Kenner, H. Scheuch, J.M. Penninger, E.F. Wagner, Epidermal JunB represses G-CSF transcription and affects haematopoiesis and bone formation. Nat. Cell Biol. **10**, 1003–1011 (2008)
21. J.E. Onyia, B. Miller, J. Hulman, J. Liang, R. Galvin, C. Frolik, S. Chandrasekhar, A.K. Harvey, J. Bidwell, J. Herring, J.M. Hock, Proliferating cells in the primary spongiosa express osteoblastic phenotype in vitro. Bone **20**, 93–100 (1997)
22. K.J. Livak, T.D. Schmittgen, Analysis of relative gene expression data using real-time qPCR and the 2(-Delta Delta C(T)) method. Methods **25**, 402–408 (2001)